Validation by PIV of the Numerical Study of Flow in the Plenum Chamber of a Swirling Fluidized Bed

Safiah Othman[1], Abas A. Wahab[1], Vijay R. Raghavan[2]

[1]*Universiti Tun Hussein Onn, MALAYSIA*
[2]*Universiti Teknologi Petronas*, *MALAYSIA*

Abstract

The primary objective of this study is to validate the numerical methods applied in the analysis of the plenum chamber in a swirling fluidized bed. The plenum chamber plays a vital role in pre-distributing the fluid evenly before it enters the distributor air gap, as maldistribution affects the performance of the fluidized bed. Comparison of the CFD predicted flow patterns and velocities calculated with the experimental data (using particle image velocimetry) are presented, and it is confirmed that good agreement is obtained.

Keywords: Swirling fluidized bed; uniformity of flow; numerical validation; experimental study; particle image velocimetry.

1. Introduction

The unique features of the fluidized bed, viz., excellent mixing capacity and high heat and mass transfer rates, are highly dependant on the quality of the fluidization, resulting from the bubbling characteristics of the fluidizing gas, which depends to a large extent on the distributor design. This is how a swirling fluidized bed featuring the inclined injection of gas to the distributor blade is of advantages [1,2].

Currently, there are plenty of investigations have been conducted on the plenum chamber in other systems such as air-cooled heat exchanger and boiler [3,4]. Although a few researches concerning the plenum chamber in a fluidized bed are also available [5,6], none are found concerning the swirling fluidized bed.

Therefore in the present work, experimental and numerical studies are carried out to investigate the aerodynamic behavior in the plenum chamber of a swirling fluidized bed. The findings are essential in designing of the plenum chamber; hence it is expected to lead to optimum performance characteristics of the whole unit. Therefore, the main objective of the study is to validate the numerical methods to be applied in the design of the plenum chamber

2. Experimental Study

A plenum chamber used in the study is shown in figure 1. It comprised a perspex plenum chamber with a tangential entry inlet pipe of 10 cm diameter and a column with 30 cm diameter and 50 cm height. The inlet pipe was slightly offset; 9 mm in radial and 5 mm in axial direction. Ambient air was directed from a blower into the column via a piping system. A flexible hose was used to transport air from the blower outlet into a long straight pipe section. The flexible hose was chosen due to its ability to tolerate misalignment as well as its capability to absorb vibration. The

long pipe is long enough to provide fully developed flow into the plenum [7]. In addition, a relatively fine screen was placed upstream of the pipe in order to homogenize the generated turbulent air stream. A 20 cm perspex flow modifying center-body of 50 cm height could be implanted at the center of the chamber. In this case, the airflow is restricted within an annulus path between the two cylinders.

(a)   (b)
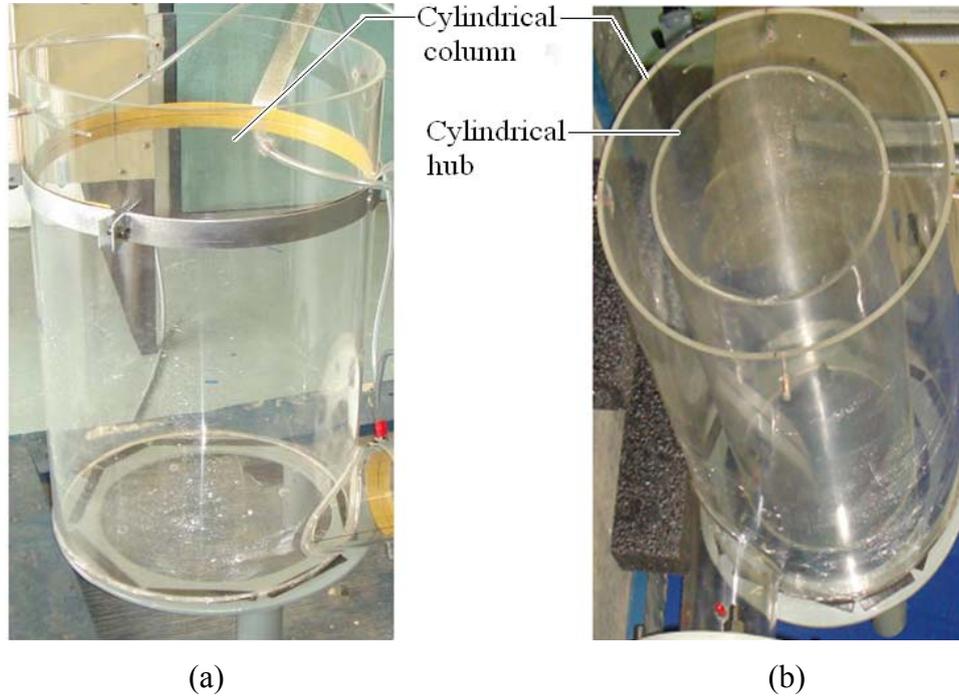
Figure 1. The plenum chamber; a) empty column; (b) cylindrical hub implanted at the center

The air flow entering the plenum was measured by a pitot static probe inserted into the inlet pipe. The pressure differential was measured by a digital manometer of resolution 1 Pa. For fully developed turbulent flow, only the air velocity at the central axis, v_c, was recorded and the mean velocity, v, was obtained using the equation 1 [8].

$$\frac{v}{v_c} = 0.817 \tag{1}$$

Particle Image Velocimetry (PIV) (figure 3.7) was used to visualize the flow and provide quantitative information about the velocity field on several horizontal and vertical planes in the plenum chamber. In these experiments, smoke of density 1.12 kg/m^3 (Aerotech SG 590) was injected into the airstream, through the gap near the blower inlet damper, into the airstream to follow streamlines. A Solo Nd:YAG laser was used to illuminate the particle suspension in the plenum chamber both vertically and horizontally. The Nd:YAG laser emit infra-red radiation the frequency of which can be doubled to 532 nm – a green wavelength. Dantec Dynamic 80C60 HiSense CCD Camera of 768×576 pixels resolution connected to a frame grabber card in a PC views the apparatus through the window at right angles to the illuminated plane. FlowManager software was used to operate the frame grabber. During the data acquisition, the PC records a sequence of images of the tracer particles. Each image is subsequently divided into interrogation windows of 64 × 64 pixels. The velocity of the flow in each window is calculated using cross-correlations between corresponding windows in successive images.

Using this technique, it is assumed that the tracer particles follow the motion of the fluid exactly; hence the displacement of the particle assembly matches the fluid displacement. The property actually measured is the distance travelled by particles in the flow within 10 ms of time

interval between successive images. This corresponds to the time delay between two laser pulses. Consequently, the instantaneous whole field velocities can be calculated from equation 2.

$$\text{speed} = \frac{\text{distance}}{\text{time}}$$ (2)

3.   Numerical Study

CFD code FLUENT had been used to analyze the flow characteristics in the plenum. Modeling and mesh generation was however performed in Gambit environment. Air has been taken as the fluid medium. Figures 2 (a-c) show the schematic diagram of the model. The plenum chamber however, is actually of 50 cm height. The extension of 50 cm in height of the numerical domain is necessary for two reasons. First, a plenum is always followed by a system, for the current study for instance, the fluidized bed column. Therefore, extending the domain will resemble the actual scenario. Second, the absence of flow extension will cause unrealistic, excessive backflow at the outlet. However, very long length of extension will equalize the velocity profile. The effects will propagate upstream, but not much. A long length will also severely increase the computational domain. Therefore, we seek for a reasonable middle solution. 50 cm extension length, which is similar to the actual plenum height was chosen on the basis of research studied by Depypere et al [9].

For the simulation purpose, the 3-D equations in cylindrical coordinates form (equations 3 to 6) have been solved numerically for a Newtonian, incompressible fluid.

Continuity Equation

$$\frac{1}{r}\frac{\partial(rv_r)}{\partial r} + \frac{1}{r}\frac{\partial v_\phi}{\partial \phi} + \frac{\partial v_z}{\partial z} = 0$$ (3)

Conservation of Momentum Equations

$$v_r \frac{\partial v_r}{\partial r} + \frac{v_\phi}{r}\frac{\partial v_r}{\partial \phi} - \frac{v_\phi^2}{r} + v_z \frac{\partial v_r}{\partial z} =$$

$$-\frac{1}{\rho}\frac{\partial p}{\partial r} + \frac{\mu}{\rho}\left\{ \frac{\partial}{\partial r}\left(\frac{1}{r}\frac{\partial}{\partial r}[rv_r] \right) + \frac{1}{r^2}\frac{\partial^2 v_r}{\partial \phi^2} - \frac{2}{r^2}\frac{\partial v_\phi}{\partial \phi} + \frac{\partial^2 v_r}{\partial z^2} \right\}$$ (4)

$$v_r \frac{\partial v_\phi}{\partial r} + \frac{v_\phi}{r}\frac{\partial v_\phi}{\partial \phi} + \frac{v_r v_\phi}{r} + v_z \frac{\partial v_\phi}{\partial z} =$$

$$-\frac{1}{r\rho}\frac{\partial p}{\partial \phi} + \frac{\mu}{\rho}\left\{ \frac{\partial}{\partial r}\left(\frac{1}{r}\frac{\partial}{\partial r}[rv_\phi] \right) + \frac{1}{r^2}\frac{\partial^2 v_\phi}{\partial \phi^2} + \frac{2}{r^2}\frac{\partial v_r}{\partial \phi} + \frac{\partial^2 v_\phi}{\partial z^2} \right\}$$ (5)

$$v_r \frac{\partial v_z}{\partial r} + \frac{v\phi}{r}\frac{\partial v_z}{\partial \phi} + v_z \frac{\partial v_z}{\partial z} =$$

$$-\frac{1}{\rho}\frac{\partial p}{\partial z} + \frac{\mu}{\rho}\left\{ \frac{1}{r}\frac{\partial}{\partial r}\left(r\frac{\partial v_z}{\partial r} \right) + \frac{1}{r^2}\frac{\partial^2 v_z}{\partial \theta^2} + \frac{\partial^2 v_z}{\partial z^2} \right\}$$ (6)
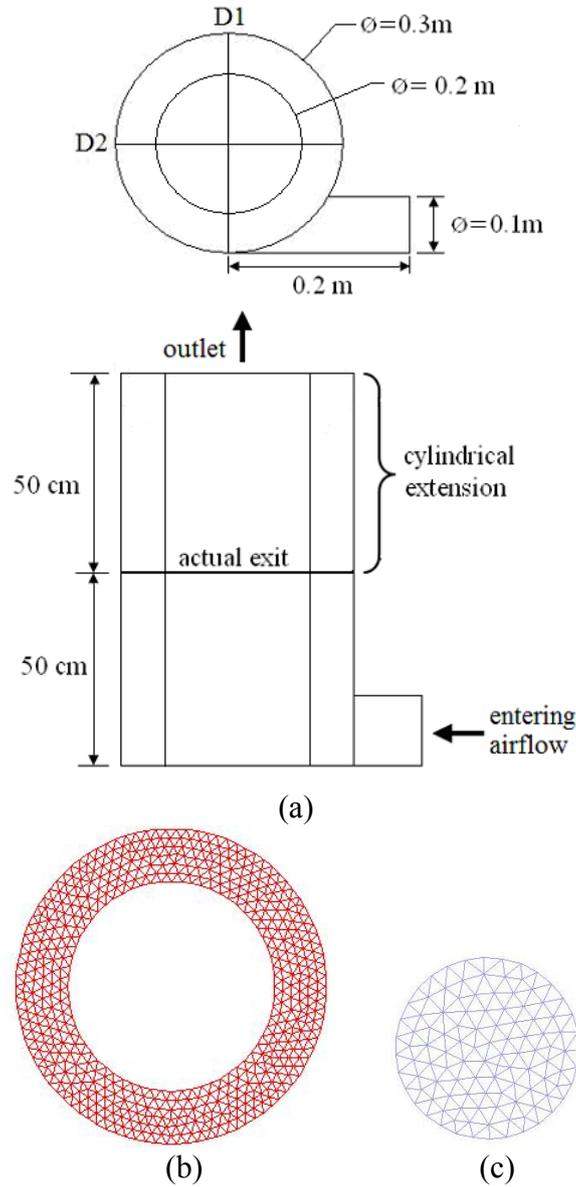
Figure 2. (a) Domain; (b) meshes on the outlet plane; (c) meshes on the inlet plane

The air inlet was modeled as a velocity inlet boundary condition of 12.3 m/s for empty column and 12.8 m/s for column with hub. The air outlet was modeled as a pressure outlet of 1.01325bar (atmospheric pressure). No slip wall conditions were applied. Air has been taken as the fluid domain, while the cylindrical hub taken as a solid medium.

Simulations were performed using double precision solver in order to capture small gradients and minimize round-off error. Steady-state segregated implicit solver and Reynolds-Averaged Navier-Stokes (RANS) Equations Models with standard wall treatment were applied to simulate the turbulent flow. Four different RANS turbulence models were considered in the present study: standard k-ε, Realizable k-ε, RNG k-ε and Reynolds stress model (RSM).

A standard discretisation scheme was used for the continuity equation while a first-order upwind scheme was used for both the turbulence kinetic energy equation and the turbulence dissipation rate equation. To reduce numerical diffusion, a second-order upwind scheme was selected for the discretisation of the momentum equations. The SIMPLE algorithm was then applied to solve the pressure-velocity coupling algorithms. A solution was considered converged (1) when the scaled residuals had dropped three orders of magnitude for all simulated variables and (2) when the conservation of overall mass balance through domain boundary exceeds 99%.

A grid independence study was also conducted. Applying the most recommended non-dimensional distance from the wall, $y^+ \approx 30$ gave the finest mesh to be 7 mm. Finer mesh was not to be expected to lead to accurate results. Therefore a grid independence study was carried out for three mesh interval sizes of 7 mm, 8 mm and 9 mm which generated 1 003 092, 830 807 and 571 526 mesh volumes respectively.

D1 and D2 are two orthogonal diameters on the column outlet surface as shown in figure 3. Referring to the overlapping of lines on D1 and D2 for mesh sizes of 7 mm and 8 mm in figures 4 (a and b), the mesh interval of 7 mm for the whole air domain has been chosen. It is evident that finer mesh will not provide much different results.
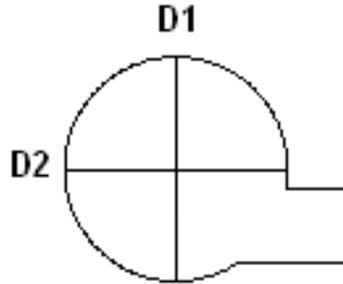
Figure 3. Two orthogonal diameters on the outlet surface

| (a) | (b) |
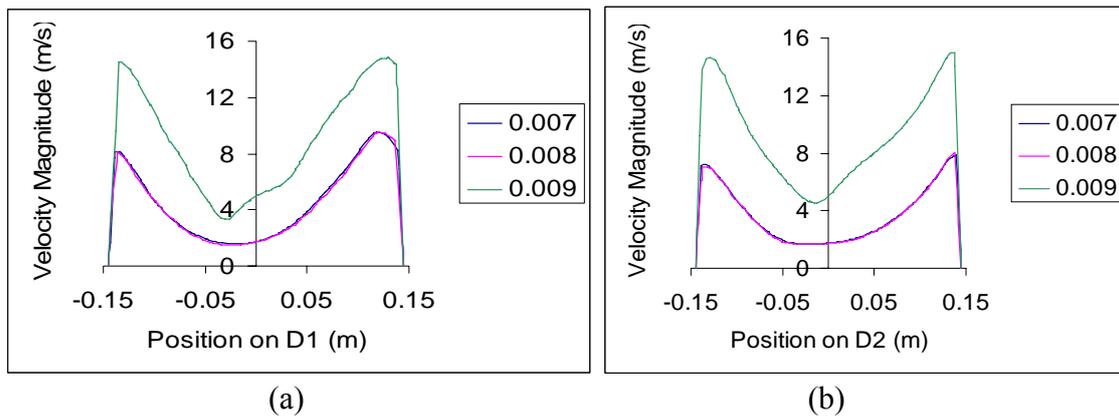
Figure 4. Velocity for various mesh sizes (m); (a) D1; (b) D2

4.   Results and discussion

Similar setting of the blower inlet damper provided different air flow rate into the plenum chamber for experimental set-up with and without a cylindrical hub. Measuring the pressure differentials across the pitot static probe, $p_0 - p_\infty$, and substituting their average into Bernoulli's equation 7 gave results as presented in table 1.

$$p_0 - p_\infty = \frac{1}{2}\rho v_\infty^2 \tag{7}$$

TABLE 1: EXPERIMENTAL RESULTS

Plenum chamber	$p_0 - p_\infty$ [Pa]	v_c [m/s]	v [m/s]
Empty plenum	127	15.06	12.3
Cylindrical hub	137	15.67	12.8

4.1. Flow Visualization

The following are the 2D air flow vector in the plenum chamber as captured using both PIV apparatus and FLUENT simulations. Similar flow patterns for both approaches were obtained, thus proving the reliability of the numerical methods applied in this study.

The flow vectors are essential in understanding the general aerodynamics in the test unit. Figures 5 to 7 (a and b) are the 2D velocity vectors on the plenum horizontal plane at three different heights labeled as top, mid and bottom in figure 8. Figures 10 (a and b) consequently, are the velocity vectors on a vertical plane intersecting the column central axis as demonstrated in figure 9. The plane is labeled as plane 1.

(a)   (b)
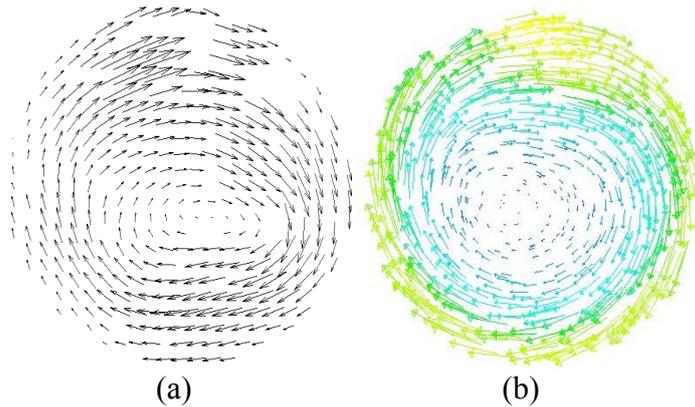
Figure 5. Velocity vector on the top plane; (a) PIV; (b) CFD

(a)   (b)
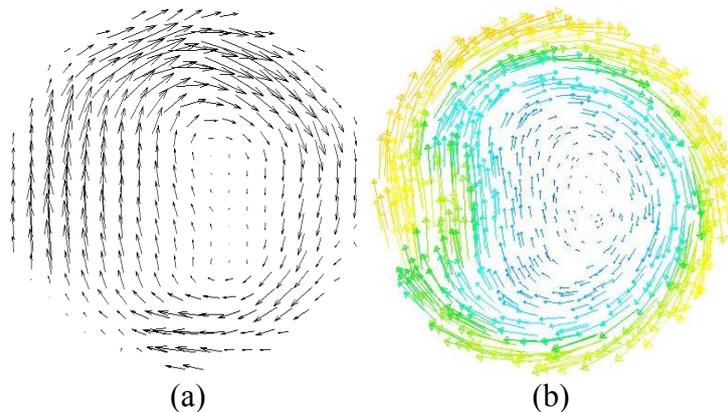
Figure 6. Velocity vector on the mid plane; (a) PIV; (b) CFD

(a)   (b)
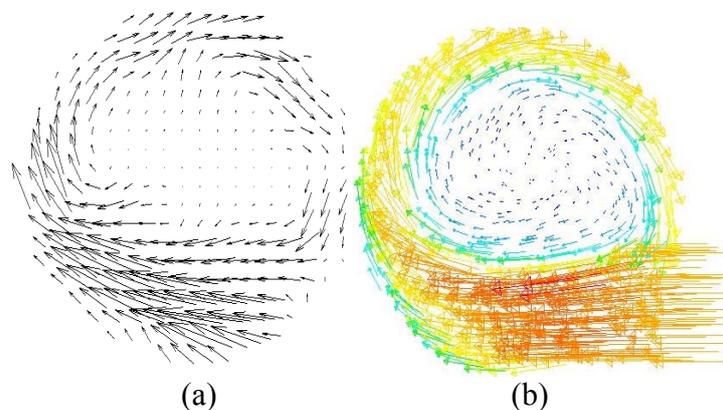
Figure 7. Velocity vector on the bottom plane (a) PIV; (b) CFD
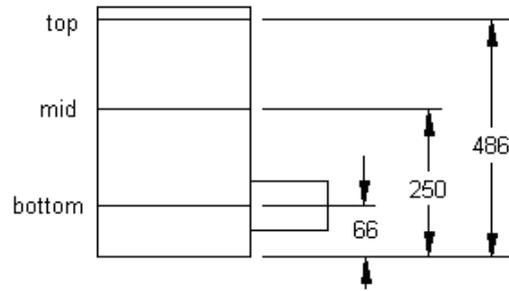
Figure 8. Three plenum heights (mm)

Figure 9. Plane 1

(a)   (b)
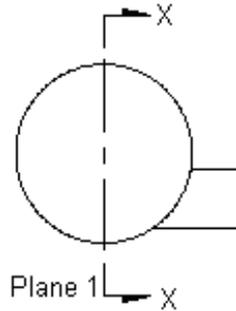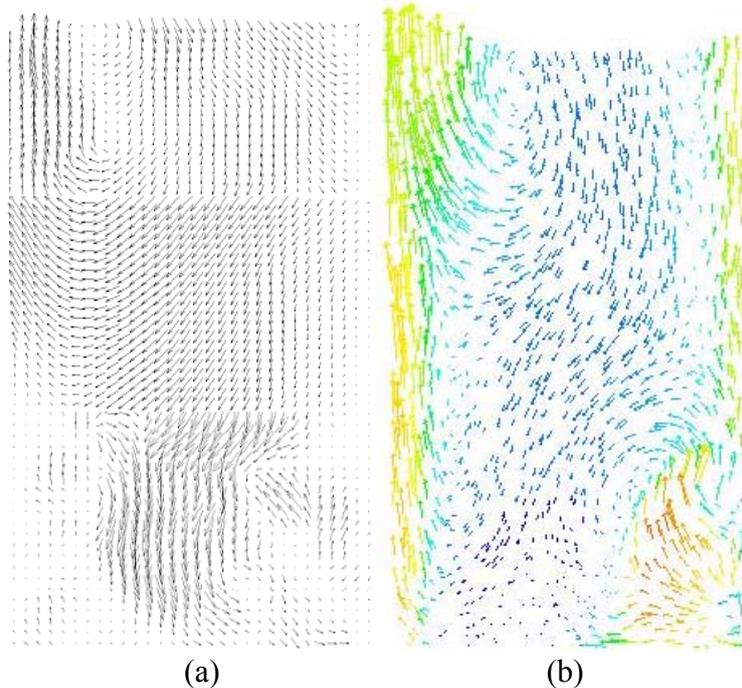
Figure 10. Velocity vector on plane 1; (a) PIV; (b) CFD

The velocity vectors (figures 5 to 7) show that the swirling flow dominated a major portion of the chamber except near the centre of the column, where the axial velocity turned out to be the most significant component. On the bottom plane, the dominant inlet velocity near the column entry was as expected. On the top and mid plane however, it was interesting to note that highest velocity magnitude occurred near the end opposite to the air entrance into the column. This could be physically explained by air being forced to flow upward in a swirling motion, toward the only exit.

The significance of axial velocity component near the centre of the column is enhanced by the vertical flow visualizations in figures 10 (a and b). In addition, it verifies that reversed

flow do take place in the centre region, however in the direction shifted to one of the wall sides. This explains the existence of the other two velocity components in this region.

Velocity vectors for the column with a cylindrical hub introduced at the centre also verify close agreement in flow patterns between both experimental and numerical study (figure 11). The numerical methodology applied thus has again been validated.

However, spurious vectors and missing vectors are as expected from PIV technique; occur for a variety of reasons. These may be associated with the optical conditions, for example, reflection of a light source from a glass surface. In fact, the light deflection on the wall of the plenum contributes to worse quality of vertical images (figures 10 a and b) compared to the horizontals (figures 5, 6, 7 and 11). In homogeneity of the tracer particles, will also cause erroneous results. Motion of trace particles into or out of the illuminated plane may cause problems.

(a)   (b)
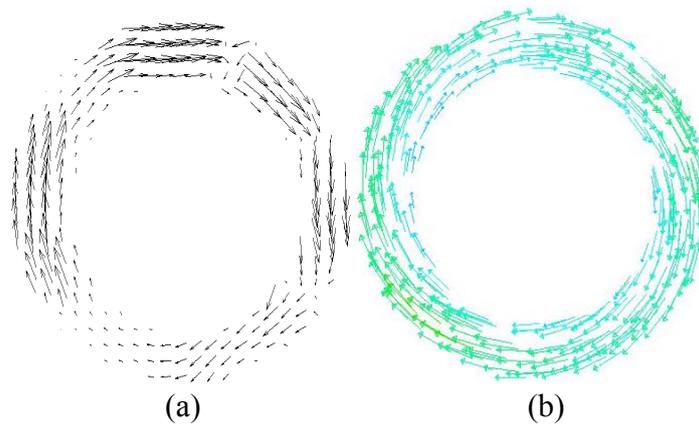
Figure 11. Velocity vector on the top plane; (a) PIV; (b) CFD

4.2. Turbulence models

In addition, computational software could calculate the velocity of the flow vectors above. Each arrow could be resolved into two velocity components. These experimental data has been used to validate the numerical approaches applied in the current study.

Figures 12 (a to d) show the comparison between experimental (PIV) results and simulations using four turbulence models for empty plenum chamber. Four constituent graphs present the profile of u and v velocity components on the two orthogonal diameters D1 and D2 on the plenum chamber outlet plane. The similar plots for plenum chamber with a cylindrical hub are shown in figures 13 (a to d).

From these resulting outputs, it is evidence that a number of turbulence models provide different results. Although some give distinct data compared to the experimental, the RNG k-ε and RSM do present reasonable flow patterns weigh against PIV results. However, through a close observation, the Reynolds stress model (RSM) has been chosen as the most suitable model that gives the closest results compared to the experimental.

4.3. Quantitative validation

Figures 14 (a to d) are the enhanced plots comparing the experimental (PIV) results with simulations using RSM model for empty plenum chamber. The similar plots for plenum chamber with a cylindrical hub are shown in figures 15 (a to d).

These figures verify the satisfactorily qualitative agreement between numerical and experimental data. However accessing the discrepancies quantitatively is essential. Therefore, the percentages of deviation (%) between CFD and PIV results for each velocity components

(u and v) on both diameters D1 and D2 were calculated and tabulated in table 3. These components are named cases 1 to 8 according to their sequence in figures below.

Engineering is the art of coping with uncertainty and in exactitude. The statistical standard deviation was used to determine the deviation between experimental and numerical results. The percentages of deviation obtained as tabulated in table 1 give an average of 15.6 % discrepancy, which is reasonable in highly complex flow situations as the present one.

TABLE 3: COMPARISON BETWEEN CFD AND PIV RESULTS

Case	Hub	Diameter	Velocity Component	Percentage of deviation (%)
1	None	D1	u	18.3
2	None	D1	v	20.5
3	None	D2	u	13.4
4	None	D2	v	16.5
5	Cylindrical	D1	u	19.2
6	Cylindrical	D1	v	8.2
7	Cylindrical	D2	u	16.1
8	Cylindrical	D2	v	12.3

(a)

(b)

(c)

(d)
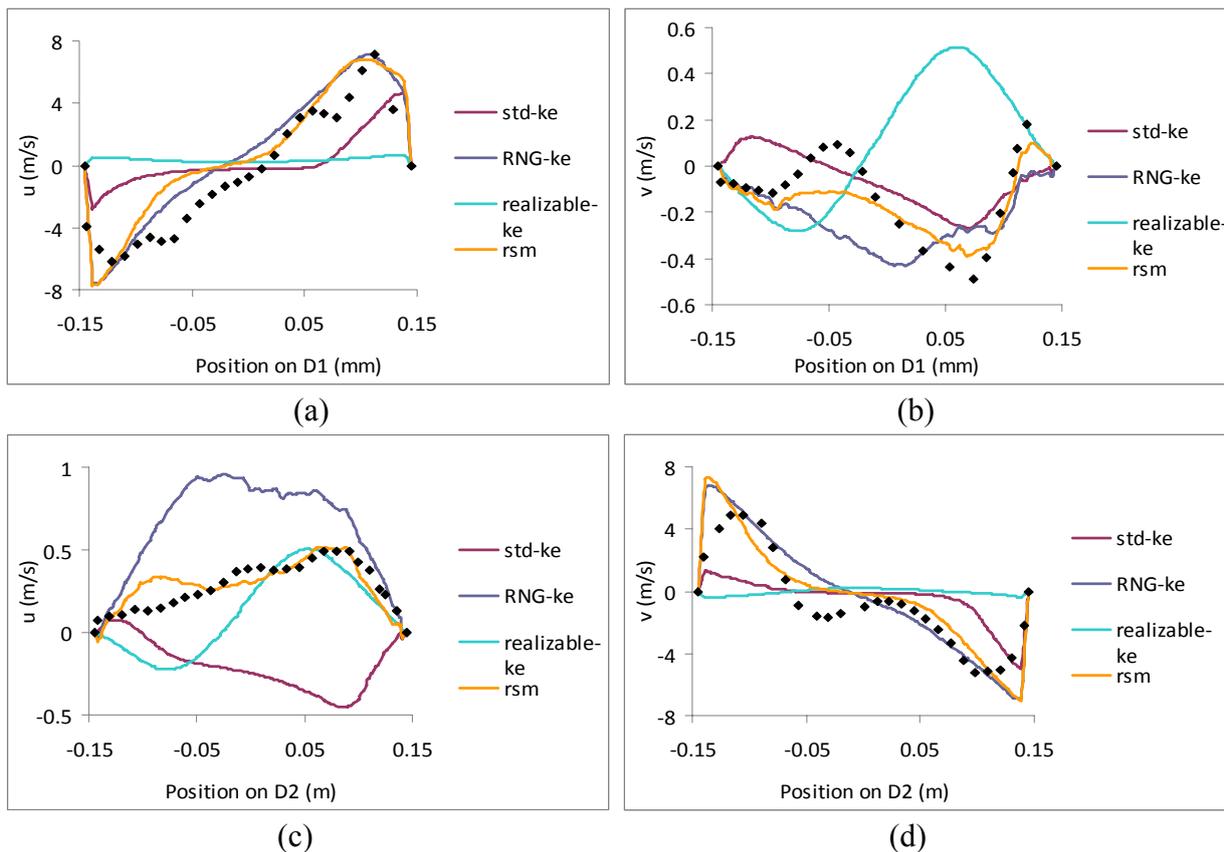
Figure 12. Comparing PIV results with various turbulence models for empty plenum

(a)

(b)

(c)

(d)
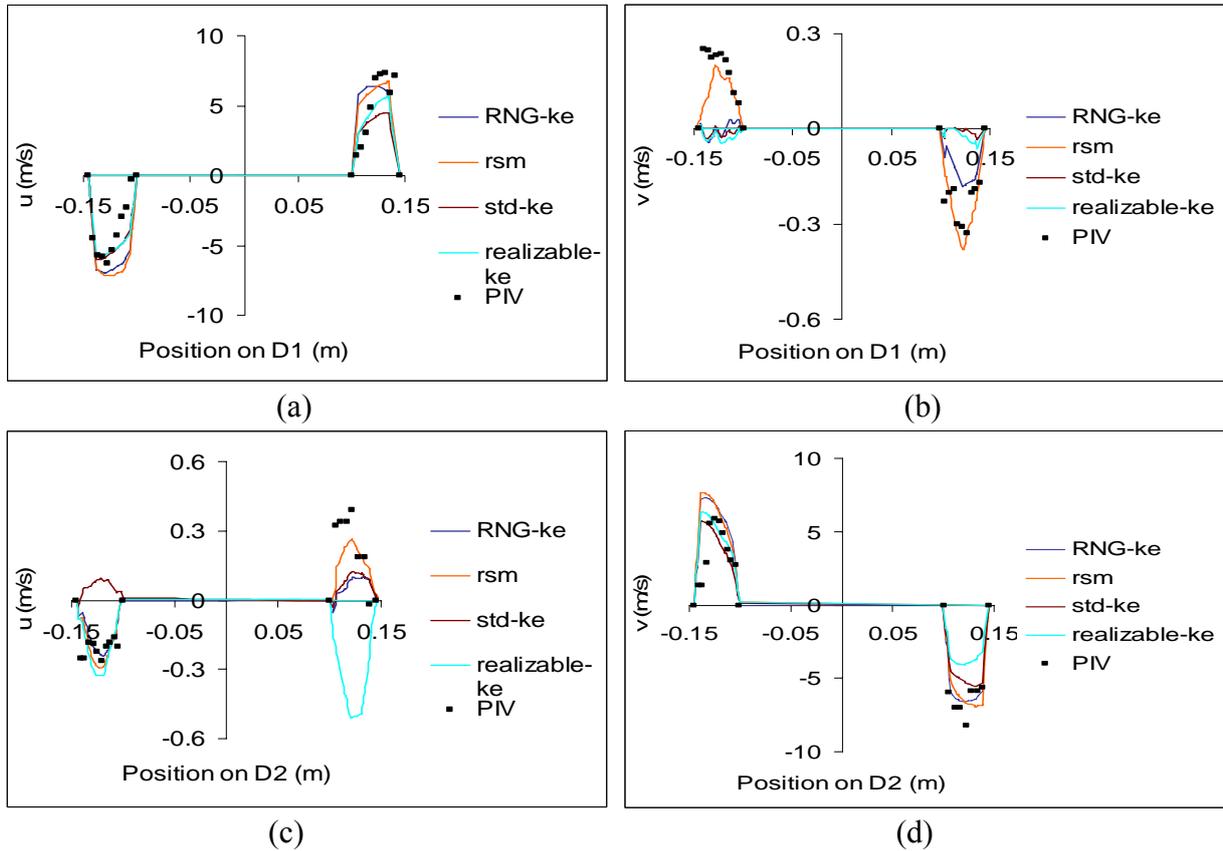
Figure 13. Comparing PIV results with various turbulence models for plenum with a cylindrical hub

(a)

(b)

(c)

(d)
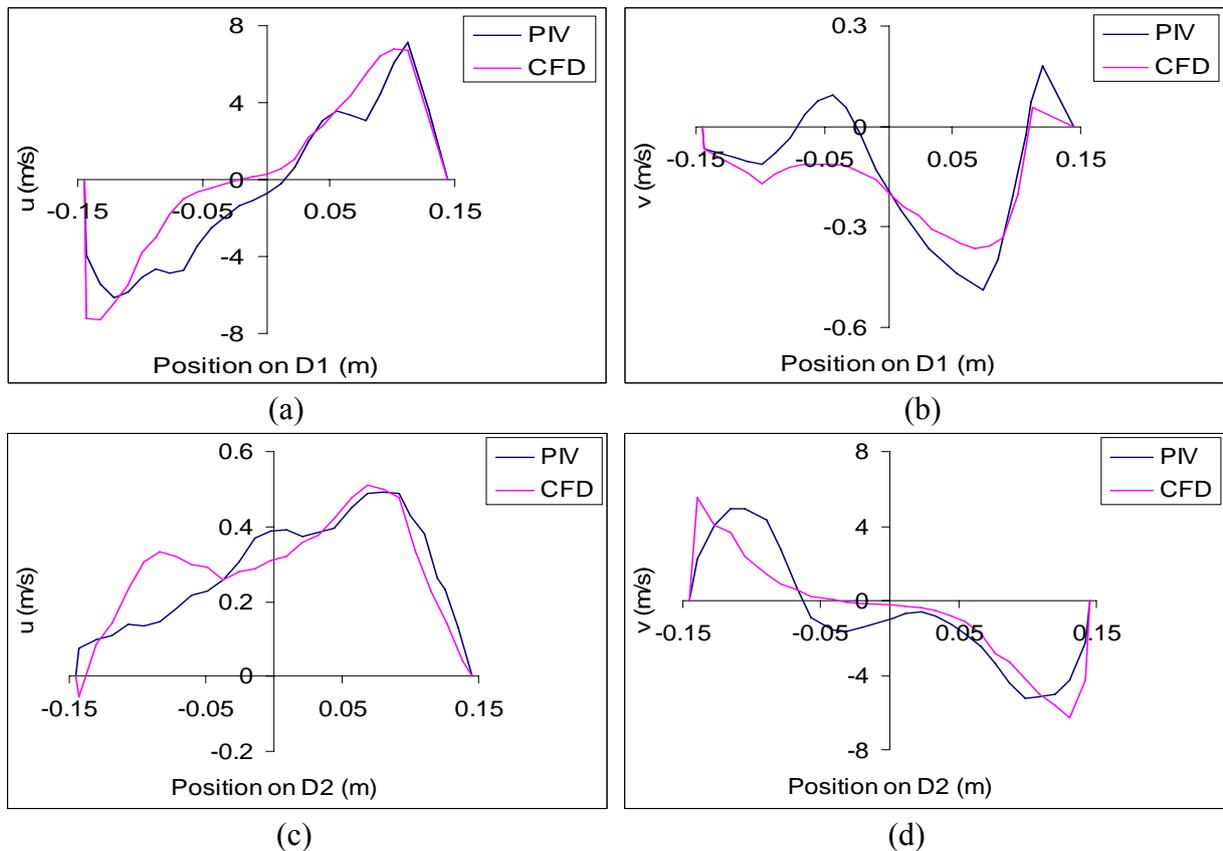
Figure 14. Comparing PIV results with simulation (RSM) for empty plenum
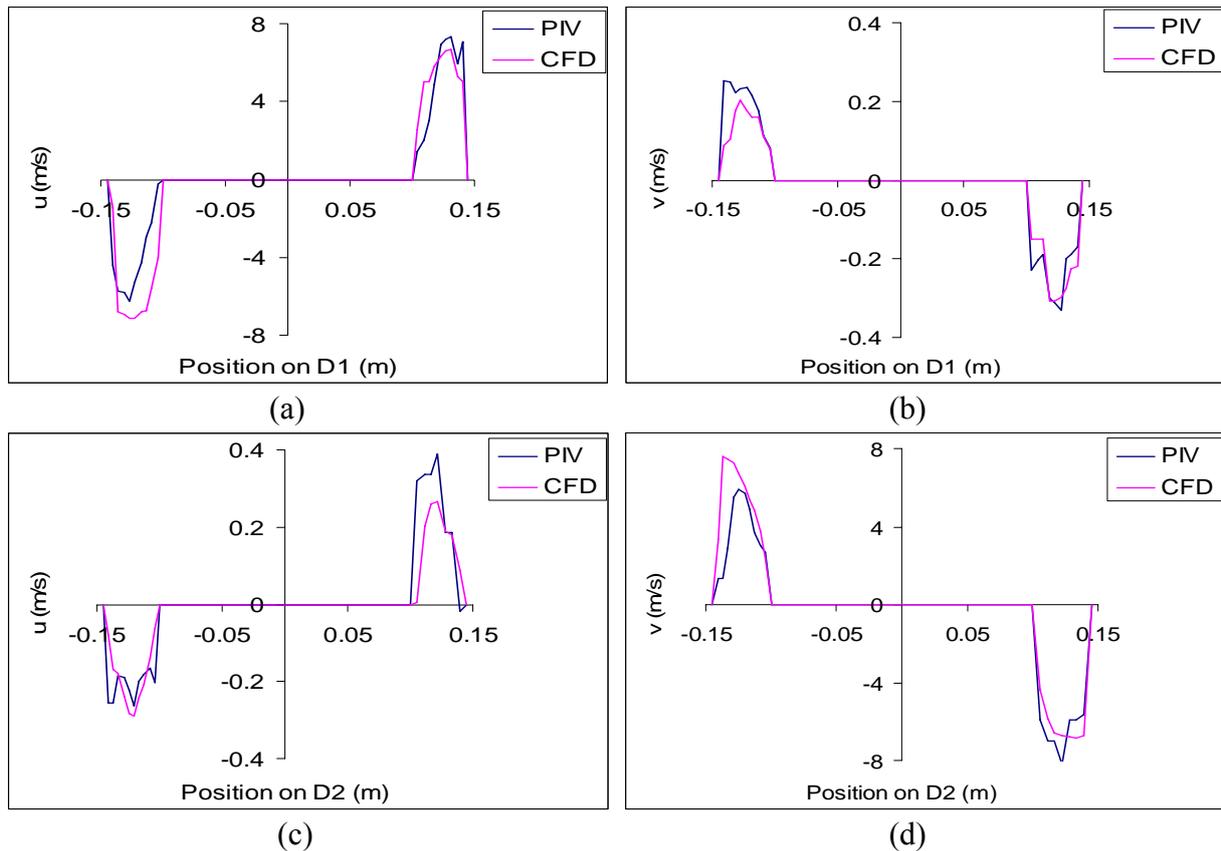
Figure 15. Comparing PIV results with simulation (RSM) for plenum with a cylindrical hub

5. Conclusion

The objective of this study, which is to validate the numerical methods applied in the current work have been achieved. Good agreements between the predicted flow patterns and calculated velocities with the experimental data are obtained. 15.6 % of average deviation between the two approaches is reasonable in view of the extremely complex nature of the flow in the plenum chamber. It confirms that the verified numerical methodology is usable in the future design of the plenum chamber in a swirling fluidized bed.

ACKNOWLEDGEMENT

Nomenclature

p	pressure	(Pa)
ρ	density	(kg/m^3)
μ	dynamic viscosity	(Pa s)
r, ϕ, z	cylindrical polar coordinates	
x, y, z	cartesian coordinates	
v	velocity	(m/s)
v_r, v_ϕ, v_Z	component of velocity vector	(m/s)

References

[1] Shu, J., *et al., Sintering and ferrite formation during high temperature roasting of sulfide concentrates,* Can. Metall. Quart, 1999. **38:** p. 215 – 225.

[2] Dodson, C., Torbed or not Torbod?. Chemical Engineer, London. 1996.

[3] Rubin, F. L., *Design of air-cooled heat exchangers,* Chemical Engineering, 1960. **68:** p. 91 – 96.

[4] Meyer, C. J. and Kroger, D. G., *Plenum chamber flow losses in forced draught air-cooled heat exchangers,* Applied Thermal Engineering, 1998. **18:** p. 875 – 893.

[5] Senadeera, W., *et al., Methods for effective fluidization of particulate food materials,* Dry. Technol*., 2000. **18*** : p. 1537 – 1557.

[6] Sathiyamoorthy, D. and Horio, M., *On the influence of aspect ratio and distributor in gas fluidized beds*. Chem. Eng. J., 2003. **93**(2): p. 151-161.

[7] Sherman, F., Viscous flow. McGraw-Hill. New York. 1990.

[8] Fox, R. W. and McDonald, A. T., Introduction to fluid mechanics. Wiley. New York. 1994.

[9] Depypere, F. et al., *CFD analysis of air distribution in fluidised bed equipment,* Powder Technology, 2004. **145**: p. 176 – 189.